

STRUCTURAL INTEGRITY EVALUATION OF A BALL MILL

Julio R. B. Cruz

CDTN/CNEN, Caixa Postal 941, 30.123-970, Belo Horizonte, MG, Brasil
jrbc@cdtn.br

Roberto R. D. da Silva

Control Test Engenharia Ltda., Rua José Cláudio Sanches, 330, CEP: 30.855-445, Belo Horizonte, MG, Brasil
ctest@uai.com.br

Abstract. *The purpose of this paper is to describe the structural integrity assessment of a ball mill in view of the presence of cracks that appeared in circumferential welded joints during its operation. The work consisted of the following steps: (a) finite element stress analysis; (b) conventional fatigue analysis; (c) estimation of critical crack sizes in the welded joints; and (d) residual life estimation considering fatigue crack growth as the basic degradation mechanism. The results of the stress, fatigue and fracture mechanics analyses are presented, along with the main conclusions taken from the study.*

Keywords. *structural integrity, fracture mechanics, fatigue, crack growth, ball mill*

1. Introduction

This work was motivated by the fact that a number of cracks were detected in the circumferential welded joints of a ball mill used in the mineral industry. The mill went through a repair process in which the failed welds were removed and a new replacement weld of several passes was put in place. Thus, the cracks were eliminated and the welds had their shape and finish improved. This process was stress relieved by post welded heat treatment. After all this recovery process, the mill was put back in operation, but two main questions remained, which comprise the basic objectives of the present study. These are: what are the critical crack sizes in the welded joints and what would be the mill residual life in case new cracks appear.

Ball mills are grinding equipment in which the grinder bodies are steel or cast iron spheres (balls) resistant to abrasion. Typically, a ball mill is a horizontal rotating cylinder that is set in motion by a drive system composed of gear and pinion. Mineral concentrates and, normally, water are fed in one extremity and the final product (a mixture of water and ground mineral, called pulp) is discharged at the other extremity of the mill. The mill structure consists of the main rotating elements, namely, the trunnions, heads, shell sections, and connections between these components. These components are indicated in Fig. (1). The cylindrical screen at the right end of the mill, called trommel, is used to remove any material (balls fragments, mineral, etc.) above a certain size. Another important component is the liner, set up on the inner surfaces with which the pulp gets in touch, used to protect the shell body against wear and, consequently, to maintain the structural integrity of the grinding compartment. A secondary function, not less important, of the liner is to transmit energy to the internal charge. Regarding the type of material, the liner can be metallic or rubber made.

There are two main types of ball mills according to the way the pulp is discharged: overflow and grate ball mills (Taggart, 1945). The mill analyzed in this work was originally an overflow mill, but after a certain time of operation it was transformed into a grate type mill. Also there was a replacement of the metallic liners with rubber liners. As these changes strongly influence the total charge and the way this charge is distributed over the internal surface of the mill, two different configurations were studied in this work, from now on referred here as *original configuration* and *current configuration*.

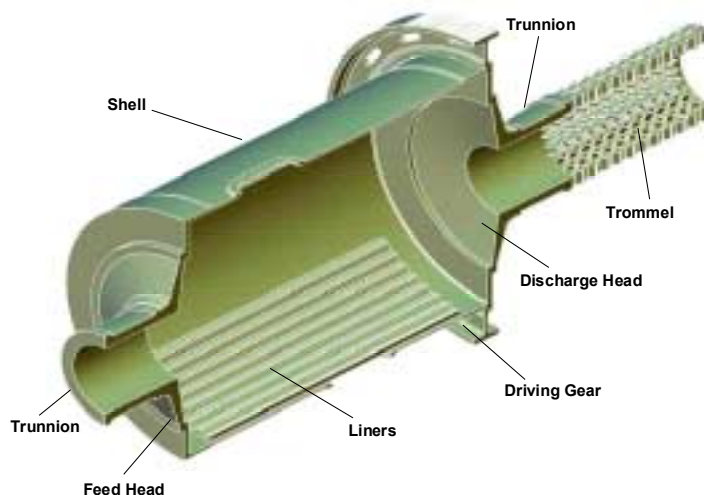


Figure 1. Main components of a ball mill.

2. Stress analysis

2.1. Finite element model

Static linear elastic finite element analyses were carried out to obtain the stress distribution over the mill. To reflect the actual structural behavior of the mill and to enable a detailed evaluation of non axisymmetric features, a complete 3D solid finite element model, containing approximately 120,000 elements, was developed. The analyses were performed with ANSYS (2001). The mill parts were modeled with SOLID45 element, defined by eight nodes, with three degrees of freedom at each node (translations in x, y, and z directions). A node at the center of each trunnion bearing was connected by “soft” link elements (using LINK8 elements) to all nodes at the respective bearing surface and was fixed to remove rigid body motion. A general view of the model is shown in Fig. (2).

The individual action of the ore, pulp and ball charge components in the mill is difficult to be modeled explicitly. Also, the exact effect of mill liners on the mill behavior is not easily modeled because of the numerous discontinuities between the liner components, and between the liner components and the mill structure. Hence, it is necessary to model the overall loading effect and the overall effect of mill liners in a simplified manner. Considering that these global effects cannot be established with a good degree of precision, the accuracy of a finite element analysis of the mill can only be guaranteed if some site monitoring is done to ensure that the actual stress ranges measured on site agree with those predicted by the analysis model. In this work, strain gage measures on different points of the mill external surface were previously obtained. Most of the measures were performed with the mill in operation, using a remote data acquisition system. The strain gage data were then used to calibrate the finite element model.

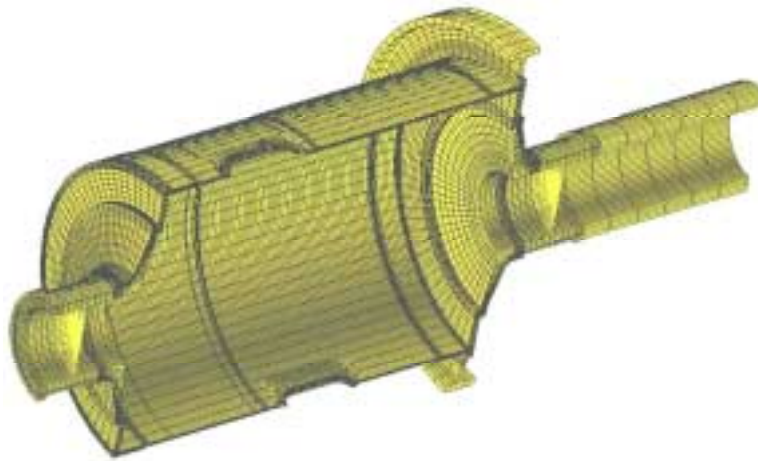


Figure 2. Longitudinal cut of the finite element model.

2.2. Loading

The loading includes the structure weight and the effect of gravity and of mill rotation on the internal charge (balls + ore + pulp). The additional weight of the liners was accounted for by increasing the material densities in the appropriate areas. The internal load, for the original and current configuration, is represented schematically in Fig. (3).

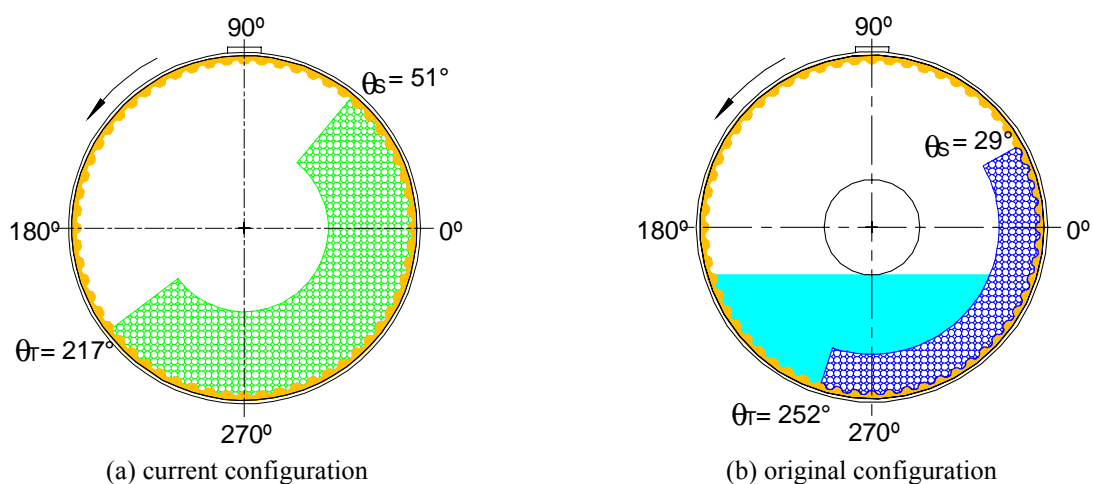


Figure 3. Load schemes for the current and original configurations of the mill.

The two key points which define the charge position are the toe (θ_t) and the shoulder (θ_s), as shown in Fig. (3). These angles are calculated using empirical equations that correlate the main operational parameters, such as fractional mill filling, fraction of theoretical critical speed and mill type (Napier-Mun et al, 1999). For this work, those fractions were, respectively, 15% and 70% for the original configuration, and 40% and 70% for the current configuration.

The internal charge loading was applied through the use of SURF154 elements. In the case of the load produced by the balls and ore, these elements simulated an added mass distributed on the mill shell, comprising the area between the angles of load dynamic equilibrium. The load relative to the pulp was applied as a hydrostatic pressure. Also, a hydrostatic pressure was applied on the external surface of the trunnion feed and discharge end bearings. This pressure was calculated as a function of the reaction forces due to the other loads computed in a first pass calculation.

2.3. Results

The most critical regions in the mill are the shell to end plate welds, referred here as welded joints C1 and C6, respectively. The deformed shape of the welded joints C1 and C6 are presented in Fig. (4). A general view of the stress distribution over the mill is illustrated in Fig. (5). A summary of the stress results used for the fatigue and fracture mechanics analyses is presented in Tables (1) and (2) for the current and original configurations, respectively. The stress ranges were computed by the algebraic difference between the numerically greater peak principal stress and the numerically greater trough principal stress of the stress cycle. The membrane and bending stress and stress range components were determined using a linearization procedure recommended in BS 7910 (1999).

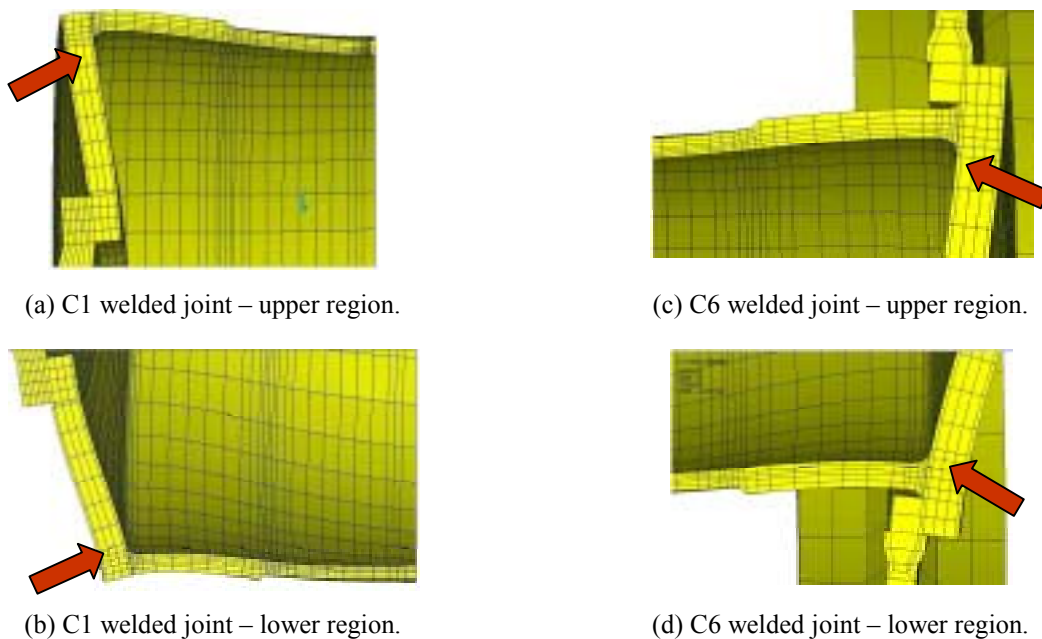


Figure 4. Scaled displacements at the welded joints C1 and C6.

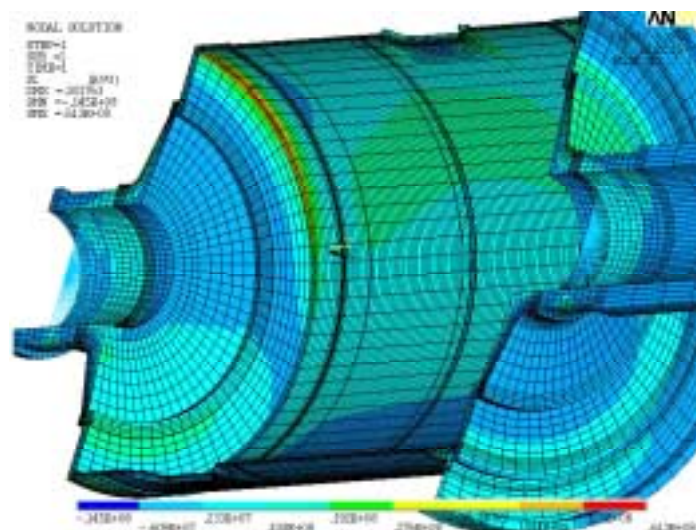


Figure 5. Longitudinal cut with a general view of the stress distribution, emphasizing the area of the welded joint C1.

Table 1. Stresses at the analysis sections – current configuration.

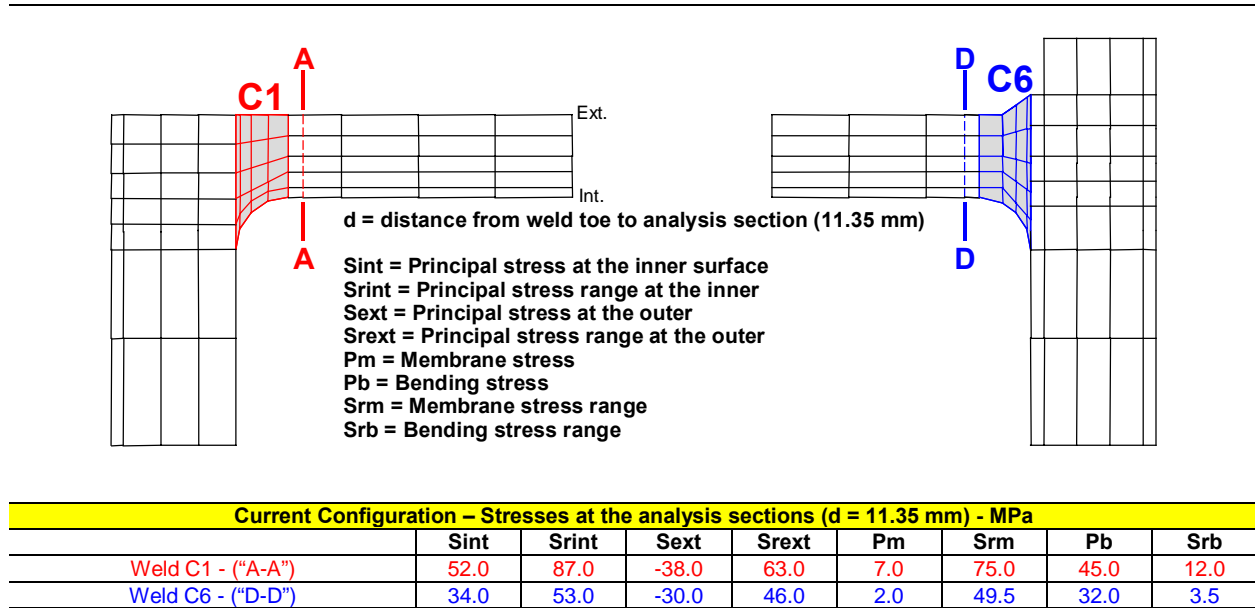
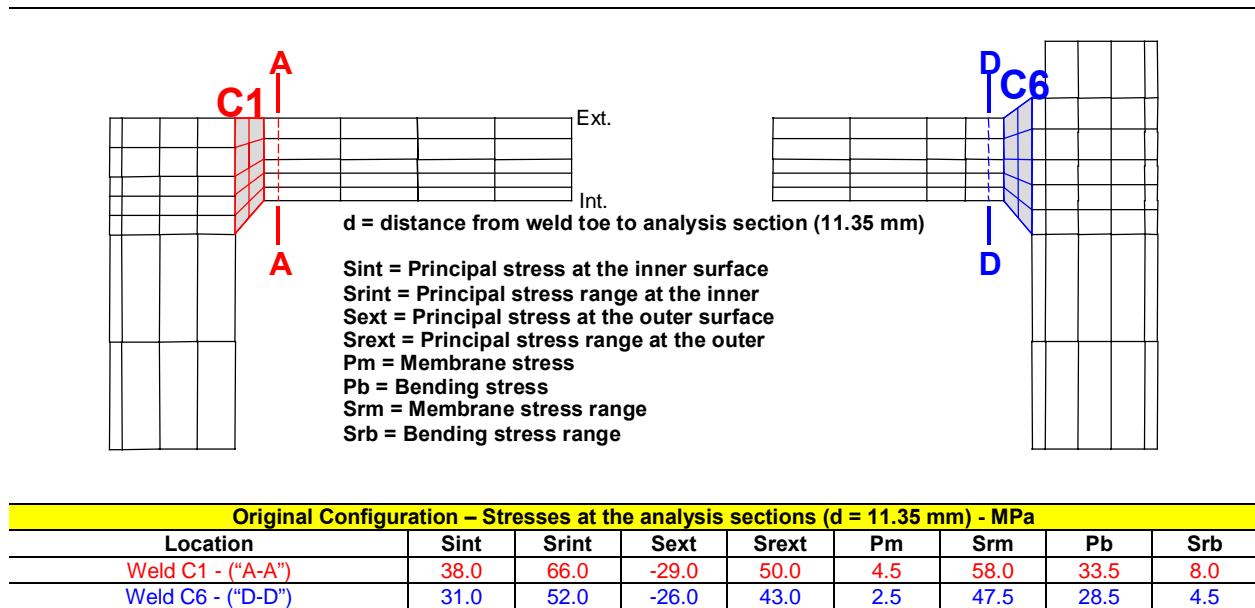


Table 2. Stresses on the analysis sections – original configuration.



3. Conventional fatigue analysis

Basically, the conventional fatigue analysis is made by comparing the applied stresses at the sections of interest, in this case the welds C1 and C6, with the allowable fatigue stresses. In the present work, the procedures and criteria of BS 7608 (1993) were used. According to this standard, for the purpose of fatigue design, the welded joints are divided into several classes, each with a corresponding design Sr-N curve (stress range versus number of cycles). The welds C1 and C6 are both full penetration butt welds. The location of potential crack initiation is at the toe of the welds joining the mill shell and the end plates. Both shell and end plates are load-carrying members. So, these welds were classified as welded joint type 8.3, class F. Their corresponding design Sr-N curve, for different nominal probabilities of failure, is shown in Fig. (6).

The number of operation cycles per year was calculated assuming a 100% operation availability, which leads to a number of cycles $N = (365 \text{ days} \times 24 \text{ hours} \times 60 \text{ minutes} \times 14.1 \text{ rpm}) = 7.4 \times 10^6$. For a 20-year life, the total number of cycles would be $N = 7.4 \times 10^6 \times 20 = 1.48 \times 10^8$ cycles. The life predictions, taking as basis the stress results presented in Tables (1) and (2), and the design Sr-N curve shown in Fig. (6), are summarized in Tab. (3).

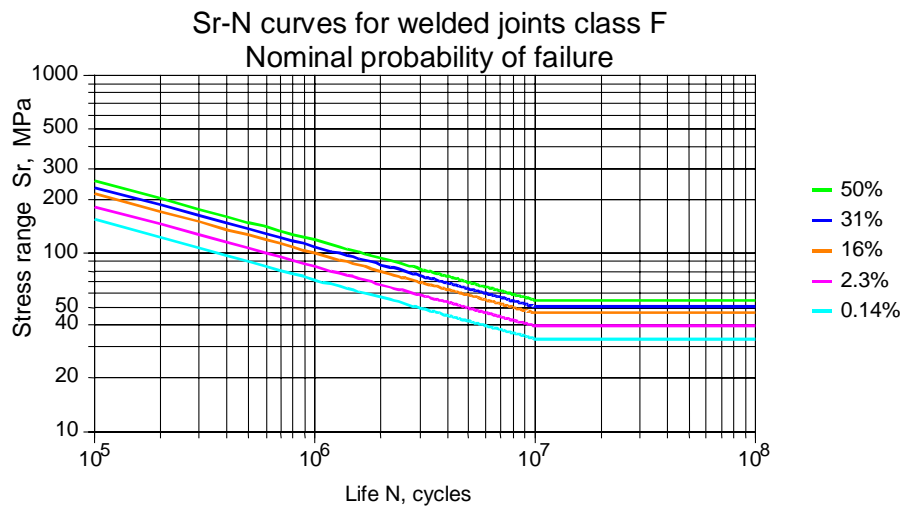


Figure 6. Sr-N curves used for evaluation of welds C1 and C6.

Table 3. Results of the fatigue analysis.

Configuration	Location	Sr (MPa)	Life for the indicated failure probability, Cycles				
			50%	31%	16%	2.3%	0.14%
Current	Weld C1	87	2.62×10^6 (4.2 months)	2.04×10^6 (3.3 months)	1.59×10^6 (2.6 months)	9.59×10^5 (1.6 months)	5.80×10^5 (0.9 months)
	Weld C6	53	-	9.02×10^6 (1.2 years)	7.01×10^6 (11 months)	4.24×10^6 (7 months)	2.57×10^6 (4 months)
Original	Weld C1	66	6.00×10^6 (10 months)	4.67×10^6 (7.5 months)	3.63×10^6 (6 months)	2.20×10^6 (3.6 months)	1.33×10^6 (2.2 months)
	Weld C6	52	-	9.55×10^6 (1.3 years)	7.42×10^6 (1 year)	4.49×10^6 (7.2 months)	2.72×10^6 (4.4 months)

4. Fracture mechanics assessments

The estimations of critical crack sizes and of fatigue crack growth life were based on the methods and criteria of BS 7910 (1999). A good history was available of the geometry of cracks observed in the welds C1 e C6 during periodic inspections performed with ultra sound technique along the operational life of the mill. Based on the details of crack length and depth, different initial crack configurations were considered for the computation of critical crack lengths and fatigue crack growth life estimations. In the present work only surface and through-thickness crack configurations were studied. Cracks should be characterized by the heights and lengths of their containing rectangles. These dimensions (see Fig. (7)) are as follows: a and $2c$ for surface cracks; a and W for long surface cracks; and $2a$ for through-thickness cracks. In all three configurations, B is the shell thickness. The corresponding stress intensity factor solutions were taken from Annex M of BS 7910.

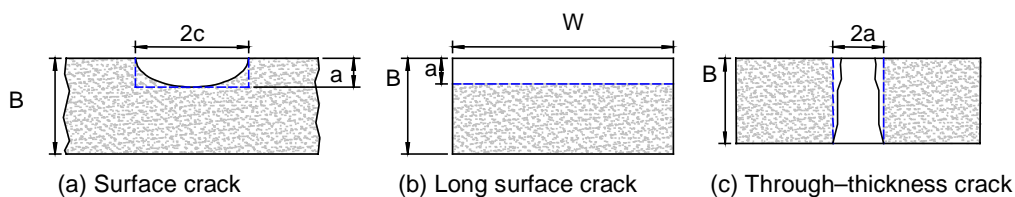


Figure 7. Required dimensions to characterize cracks.

4.1. Computational of critical crack sizes

Assessment is made by means of a failure assessment diagram (FAD). The vertical axis of a FAD is a ratio of the applied conditions, in fracture mechanics terms, to the conditions required to cause fracture, measured in the same terms. The horizontal axis is the ratio of the applied load to that required to cause plastic collapse. An assessment line is plotted in the diagram. Calculations for a given crack provide the coordinates of an assessment point. The position of this point is compared with the assessment line to determine the acceptability of the crack.

There are three levels of fracture assessment in BS 7910 (1999). The choice of level depends on the materials involved, the input data available and the conservatism required. The Level 2, named the normal assessment route, was the one chosen for the evaluations carried out in this work. Level 2 contains two methods for the definition of the failure assessment line, named Level 2A and Level 2B. In this work, Level 2A was used. This method is based on a generalized assessment line equation, not requiring a material stress-strain specific curve.

The prediction of limiting values is made through an iterative calculation in which a initial crack size is assumed and then it is increased until the point where first contact is made with the assessment line. This point corresponds to the critical crack size. Two different crack growth ways were considered for the surface cracks: one, in which the relation $a/2c$ was kept constant during crack growth, and the other, in which this relation changed during crack growth. An example of a FAD diagram, corresponding to one of the analyzed cases, is shown in Fig. (8). A summary of the results for the weld C1 is presented in Tab. (4) for the current configuration.

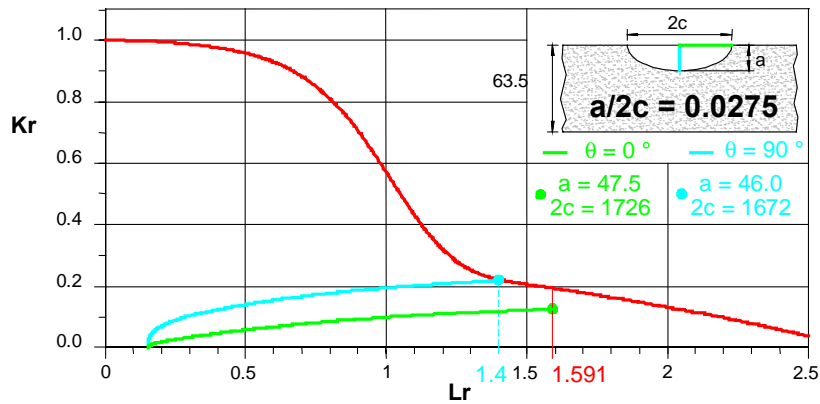


Figure 8. FAD Level 2A for surface crack – weld C1 – current configuration.

Table 4. Critical crack sizes for the weld C1 – current configuration.

Crack Geometry	Weld C1 – Current Configuration – Critical crack size (mm)		
	a/2c	$\theta = 0^\circ$	$\theta = 90^\circ$
	0.05	$a = 48.9 / 2c = 977$	$a = 49.9 / 2c = 997$
	0.0275	$a = 47.5 / 2c = 1726$	$a = 46.0 / 2c = 1672$
	0.005	$a = 44.8 / 2c = 8967$	$a = 41.5 / 2c = 8302$
	0.05 (*)	$a = 45.1 / 2c = 6420$	$a = 42.5 / 2c = 4472$
	0.0275 (*)	$a = 44.8 / 2c = 9111$	$a = 41.9 / 2c = 6507$
	0.005 (*)	$a = 42.0 / 2c = 15327$	$a = 40.5 / 2c = 14389$
		$a = 38.1$	
		$2a = 3606$	

(*) Variable relation $a/2c$ during crack growth (from $a/2c_i$ = indicated above to $a/2c_f = 0.0023$)

4.2. Fatigue crack growth evaluation

Once determined the critical crack sizes for each crack configuration, the next step is the estimation of the number of cycles for a crack of initial depth (a_i) to grow up to a final value (a_f) equivalent to the critical crack size calculated previously.

The general procedure of BS 7910 (1999) was used for evaluation of fatigue crack growth. The computation of the number of cycles is based on the integration of the equation $da/dN = A(\Delta K)^m$, which describes the relation between the rate of fatigue crack growth and the range of the stress intensity factor. The rate of fatigue crack growth is given for values above a ΔK threshold, ΔK_0 . For ΔK less than ΔK_0 , da/dN is assumed to be zero. Values of A and m depend on material and applied conditions. Recommendations are available, in BS 7910, in the form of simple laws and more precise two-stage relationships. For the latter, both the mean and mean plus two standard deviations (mean + 2SD) of $\log da/dN$ versus $\log \Delta K$ relationships for $R < 0.5$ and $R \geq 0.5$ are given, where R is the stress ratio. In this work, the crack growth laws (see Fig. (9)) were obtained using the parameters given in Tab. (5).

Table 5. Parameters used to obtain the curves of rate of crack growth.

R	Stage A				Stage B				Stage A / Stage B transition point ΔK (N/mm ^{3/2})	
	Mean curve		Mean + 2SD		Mean curve		Mean + 2SD		Mean curve	Mean + 2SD
	A	M	A	m	A	m	A	m		
< 0.5	1.21x10 ⁻²⁶	8.16	4.37x10 ⁻²⁶	8.16	3.98x10 ⁻¹³	2.88	6.77x10 ⁻¹³	2.88	363	315
≥ 0.5	4.80x10 ⁻¹⁸	5.10	2.10x10 ⁻¹⁷	5.10	5.86x10 ⁻¹³	2.88	1.29x10 ⁻¹²	2.88	196	144

- 1) Parameters values for da/dN in mm/cycle and ΔK in N/mm^{3/2}.
- 2) 2SD = 2 x Standard Deviation.
- 3) R = Stress ratio = ratio of minimum to maximum algebraic value of stress in the cycle.
- 4) The probability of survival in fatigue life calculations associated to the mean curves + 2SD is 97.7%.

According to BS 7910, the mean + 2SD laws for $R \geq 0.5$ should normally be used to assess welded components. In the case of welds C1 and C6, the stress ratio is negative, that is, $R < 0.5$. Therefore, in order to make a comparison, the crack growth curves for this condition were also considered here. The adoption of the curves for $R \geq 0.5$ is suggested by BS 7910 for conservatism and to allow for the influence of residual stresses. Table (6) gives a clear idea of the difference between the rates of crack growth as a function of the stress ratio, R. It can be observed that the difference is significantly higher for lower values of ΔK . This behavior produces also a big difference in the estimation of fatigue crack growth life.

Table 6. Comparison between the rates of crack growth as a function of the stress ratio, R.

Comparison of crack growth rates – Mean curve + 2SD			
ΔK (N/mm ^{3/2})	da/dN for $R \geq 0.5$ (mm/cycle)	da/dN for $R < 0.5$ (mm/cycle)	(da/dN for $R \geq 0.5$) / da/dN for $R < 0.5$
100	3.328 x 10 ⁻⁷	9.130 x 10 ⁻¹⁰	364.5
1000	5.631 x 10 ⁻⁴	2.955 x 10 ⁻⁴	1.905

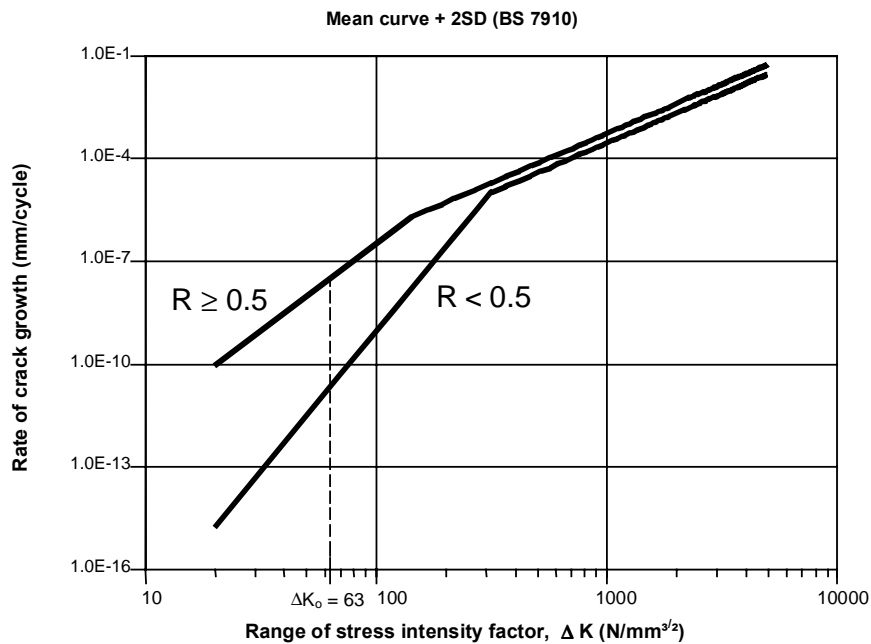


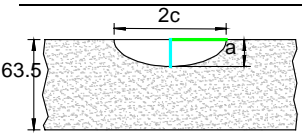
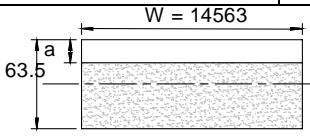
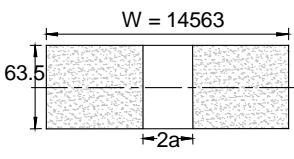
Figure 9. Rates of fatigue crack growth for $R \geq 0.5$ and $R < 0.5$.

For each crack geometry, the fatigue life was computed using the following procedure:

- (a) 1000 crack size increments were used, starting with a initial crack size value up to a crack depth of 50 mm; in the case of semi-elliptical surface cracks, the two different ways of crack growth (constant and variable relation $a/2c$) were considered;
- (b) For each crack size increment, ΔK value was calculated at the end of the increment;
- (c) The corresponding crack growth rate was then determined for each crack growth law considered (see Fig. (9));
- (d) From the previously determined crack growth rate, the number of cycles consumed for the crack size increment was obtained;
- (e) Repeating the above steps up to the critical crack size and adding the number of cycles in each increment, the total fatigue life is achieved.

The fatigue crack growth results for the weld C1 are given in Tab. (7). To assist the interpretation of the crack growth process, the crack growth life shown in Tab. (7) was divided into two parts: from 0.35 to 2.0 mm and from 2.0 mm to critical crack size (in the case of through-thickness cracks, from 10 to 200 mm and from 200 mm to critical crack size).

Table 7. Crack growth results for the weld C1.

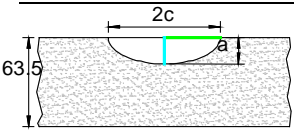
Geometry			Weld C1 – Current configuration - N° of Cycles (Time)				
			Crack growth law for R ≥ 0.5		Crack growth law for R < 0.5		
			Crack depth (mm)				
			From 0.35 - 2.0	From 2.0 - a _{crit.}	From 0.35 - 2.0	From 2.0 - a _{crit.}	
	a/2c 0.05	0°	97,638 (5 days)	344,882 (17 days)	336,973 (17 days)	660,842 (33 days)	
		90°	2.61x10 ⁶ (4.3 months)	6.57x10 ⁶ (10.8 months)	8x10 ⁶ (1.1 years)	1.25x10 ⁷ (1.7 years)	
	a/2c 0.027	0°	5.1x10 ⁸ (68.3 years)	4.2x10 ⁷ (5.7 years)	5.3x10 ¹² (7.2x10 ⁵ years)	3.8x10 ¹⁰ (5,084 years)	
		90°	1.8x10 ⁷ (2.5 years)	9x10 ⁶ (1.2 years)	2.6x10 ⁹ (344 years)	2.7x10 ⁷ (3.6 years)	
	a/2c 0.005	0°	3.7x10 ¹⁰ (5,031 years)	2.9x10 ⁹ (392 years)	5.2x10 ¹⁵ (7x10 ⁸ years)	3.7x10 ¹³ (5x10 ⁶ years)	
		90°	1.8x10 ⁷ (2.4 years)	8.5x10 ⁶ (1.1 years)	2.4x10 ⁹ (319 years)	2.3x10 ⁷ (3.2 years)	
	a/2c _i 0.05 (*)	0°	1.2x10 ⁸ (16.3 years)	1.2x10 ⁷ (1.7 years)	5.3x10 ¹¹ (7.1x10 ⁴ years)	3.8x10 ⁹ (508 years)	
		90°	2x10 ⁷ (2.7 years)	9.2x10 ⁶ (1.2 years)	2.9x10 ⁹ (385 years)	2.7x10 ⁷ (3.7 years)	
	a/2c _i 0.027 (*)	0°	5.2x10 ⁸ (70 years)	4.8x10 ⁷ (6.4 years)	5.4x10 ¹² (7.3x10 ⁵ years)	4.7x10 ¹⁰ (6,356 years)	
		90°	1.9x10 ⁷ (2.5 years)	8.6x10 ⁶ (1.2 years)	2.6x10 ⁹ (344 years)	2.3x10 ⁷ (3.2 years)	
	a/2c _i 0.005 (*)	0°	3.8x10 ¹⁰ (5,094 years)	3.1x10 ⁹ (413 years)	5.2x10 ¹⁵ (7.1x10 ⁸ years)	3.8x10 ¹³ (5.1x10 ⁶ years)	
		90°	1.8x10 ⁷ (2.4 years)	8.2x10 ⁶ (1.1 years)	2.4x10 ⁹ (319 years)	2.3x10 ⁷ (3.2 years)	
				583,463 (29 days)	280,811 (14 days)	7.8x10 ⁷ (10.5 years)	702,000 (35 days)
				From 10 - 200	From 100 - 2a _{crit.}	From 10 - 200	From 100 - 2a _{crit.}
			237,925 (12 days)	86,872 (4 days)	459,481 (23 days)	159,968 (8 days)	

(*) – Variable relation a/2c during crack growth (from a/2c_i = indicated above to a/2c_f = 0.0023).

Original configuration – simulated only for the indicated geometry.

Analyzing the behavior of the semi-elliptical surface cracks (for the several relations a/2c), it was noted that the case of variable relation a/2c during crack growth (with the initial relation a/2c = 0.005) is the one that better approximates the actual pattern of crack growth shown by the inspection data history of the mill. Thus, taking this geometry configuration as basis for the final conclusions, the fatigue lives are summarized in Tab. (8).

Table 8. Summary of fatigue crack growth life estimations.

Current configuration		Original configuration		Weld C1 – N° of Cycles (Time)			
Geometry 		$a/2c_i$ 0.005 (*) 90°		Crack growth law for $R \geq 0.5$		Crack growth law for $R < 0.5$	
				Crack depth (mm)			
				From 0.35 - 2.0	From 2.0 - $a_{crit.}$	From 0.35 - 2.0	From 2.0 - $a_{crit.}$
				1.8x10 ⁷ (2.4 years)	8.2x10 ⁶ (1.1 years)	2.4x10 ⁹ (319 years)	2.3x10 ⁷ (3.2 years)
				6.1x10 ⁷ (8.3 years)	1.8x10 ⁷ (2.4 years)	2.235x10 ¹⁰ (3,045 years)	1.18x10 ⁸ (16 years)
				Weld C6 – N° of Cycles (Time)			
				1.8 x 10 ⁸ (25 years)	3.3 x 10 ⁷ (4.5 years)	1.3 x 10 ¹¹ (18,000 years)	7.1 x 10 ⁸ (95 years)
				2.02x10 ⁸ (27 years)	3.5x10 ⁷ (4.7 years)	1.57x10 ¹¹ (21,200 years)	7.1x10 ⁸ (96 years)

(*) – Variable relation $a/2c$ during crack growth (from $a/2c_i$ = indicated above to $a/2c_f$ = 0.0023).

5. Conclusions

The main focus of this work was the welded joints between the mill shell and the feed and discharge end plates (the welds C1 and C6), considering the current configuration of the mill, that is, grate discharge and rubber liners. Additionally, in order to make some comparisons, the mill original configuration (overflow discharge and metallic liners) was also studied. The following conclusions can be taken from the study:

- The conventional fatigue analysis, based on the Sr-N design curves of BS 7908, showed that there is a high failure probability in a very short period of time, even for the original configuration of the mill, what points to a possible error in its structural design;
- The FAD analyses indicated that for all surface crack configurations (semi-elliptical and long surface), the most likely failure mode is plastic collapse;
- In the case of through-thickness cracks, the failure mode is brittle fracture;
- The through-thickness cracks grow very quickly, so in case an initially surface crack breaks through to the external shell surface, a critical failure condition of the mill could be shortly achieved;
- There is a significant difference between the life estimations as a function of the crack growth law; for welded joints, BS 7910 recommends the use of the crack growth law for $R \geq 0.5$, which leads to relatively short lives;
- The major part of fatigue crack growth life corresponds to the period in which the crack size is very small; as shown in Tab. (8), the time for a crack to grow from 2 mm (which in fact is a hardly detectable crack size) to a critical crack size is rather short.

6. References

- ANSYS Release 5.7.1, 2001, ANSYS, Inc., Canonsburg, PA, USA.
 BS 7608: 1993 - Code of practice for Fatigue design and assessment of steel structure.
 BS 7910: 1999 - Guide on methods for assessing the acceptability of flaws in metallic structures.
 Napier-Mun, T.J., Morell, S., Morrison, R.D. and Kojovic, T., "Mineral Comminution Circuits. Their Operation and Optimisation", Australia: JKMR, 1999.
 Taggart, A.F., 1945, "Handbook of Mineral Dressing. Ores and industrial minerals", New York: John Wiley & Sons, Inc.

7. Copyright Notice

The authors are the only responsible for the printed material included in his paper.